Electron Paramagnetic Resonance Line Shifts and Line Shape Changes Due to Spin Exchange between Nitroxide Free Radicals in Liquids. 3. Extension to Five Hyperfine Lines. Additional Line Shifts Due to Re-encounters

Barney L. Bales* and Miroslav Peric

Department of Physics and Astronomy and The Center for Supramolecular Studies, California State University at Northridge, Northridge, California 91330

Ileana Dragutan

Center of Organic Chemistry, Romanian Academy, 71141 Bucharest, Romania

Received: June 10, 2003; In Final Form: July 28, 2003

The work in part 2 of this series (*J. Phys. Chem. A* **2002**, *106*, 4846) is extended experimentally and theoretically to include inhomogeneously broadened nitroxide spectra consisting of five hyperfine lines due to coupling to two equivalent ^{14}N nuclei. The nitronyl-nitroxide 1-*H*-imidazol-1-yloxy-4,5-dihydro-4,4,5,5-tetramethyl-2-(*o*-nitrophenyl)-3-oxide, which is severely inhomogeneously broadened by unresolved hyperfine structure in the absence of spin exchange, is studied under conditions in which the spin-exchange frequency, ω_e, varies from near zero to more than half of the hyperfine spacing. In common with part 2 of this series, as ω_e increases we find the following: (a) each line is the sum of one absorption and one spin-exchange-induced "dispersion" line; no other terms are needed over the entire range; (b) intensity moves from the outer lines to the central line; (c) the outer lines are broadened slightly faster than predicted by perturbation theory; (d) the amplitudes of the "dispersion" components lead to a determination of ω_e; (e) the experimental line shifts differ substantially from those predicted theoretically. Items a−e are unaffected theoretically by adding unresolved hyperfine structure which inhomogeneously broadens the lines. The discrepancy in item e is addressed by including spin precession during the spin-exchange act and re-encounters of the same spins during one collision. These additions to the theory yield an additional line shift that is proportional to ω_e. From the additional shift, the time between re-encounters is estimated to be $\tau_D \sim 10^{-10}$ s which is of the correct order of magnitude as estimated from a Stokes−Einstein diffusion model. Inclusion of the effect of re-encounters in the theory may permit a deeper understanding of the collision process as a function of liquid structure.

Introduction

The possibilities of applying spin exchange between nitroxide free radicals to problems in chemistry and biology were exciting indeed during the 1960s and 1970s when the method was developing.[1] In addition to studies of collisions in homogeneous liquids, diffusion in complex fluids, which could not be studied by other methods, seemed to be an ideal application of the method. For summaries of the history and contributors to the subject, see, for example, ref 1 and the Introduction to ref 2. The enthusiasm waned after the late 1970s, basically for two reasons. First, it was learned that spin exchange was almost invariably strong; that is, $J\tau_C \gg 1$ where J is minus 2 times the exchange integral and τ_C is the mean duration of the collision. The only exceptions involved liquids of very low viscosity[3,4] and perhaps like-charged nitroxides.[5] For strong spin exchange, the spin-exchange frequency, ω_e, is independent of J so one cannot learn anything of the exchange integral. Second, although spin exchange produces many spectral changes, only line broadening was utilized in applications. A critique of the line width method appeared[6] in 1979 that showed that the separation of the line broadening effects of spin exchange and of dipolar interactions was not likely to be successful precisely for the range of diffusion coefficients of interest in biological membranes. In this paper, we continue a recent program[2,7] to show that much more quantitative information is available from the electron paramagnetic resonance (EPR) spectra than just the line widths, perhaps offering a renaissance of the method.

The generally accepted expression[1,8] describing the line shape is given by the real part of eq 1

$$G(H) = \frac{S(H)}{1 - \frac{\omega_e}{\gamma} S(H)} \tag{1}$$

where H is the magnetic field, γ is the gyromagnetic ratio of the electron, and $S(H)$ is given by

$$S(H) = \sum \frac{\rho_j}{i(H - H_j) + \gamma^{-1}[\omega_e + (T_2^{-1})_j]} \tag{2}$$

In eq 2, $i = \sqrt{-1}$ and the sum is over j, which denotes the jth resonance line in the spectrum which appears at resonance field H_j, with degeneracy ρ_j, and is characterized by spin−spin relaxation time $(T_2)_j$. In the limit of $\omega_e = 0$, eq 1 yields

* Corresponding author. E-mail: barney.bales@csun.edu. Fax: (818) 677-3234.

10.1021/jp030726s CCC: $25.00
Published on Web 10/04/2003

Lorentzian lines with peak-to-peak first-derivative line widths $\Delta H_{pp}^{L}(0)_j = 2/\sqrt{3}\gamma(T_2)_j$. Equation 1 has been derived using many approaches[1] all of which have in common the assumption of sudden collisions originally proposed by Kivelson.[9] See p 56 of ref 1 for a detailed discussion of the assumption. We note that neither spin precession during the collision act nor re-encounters of the same spins are properly included in eq 1.

The usual approach[1] has been to approximate eq 1 in two limits. In the slow exchange limit, $\omega_e/A\gamma \ll 1$, where A is the ^{14}N or ^{15}N hyperfine spacing in gauss, the lines broaden, shift, and change shape. Perturbation theory yields expressions relating these phenomena to ω_e. In the opposite limit, the lines merge into a single line which narrows and ω_e may be extracted from the line width.[1]

Thus, as things stood more than 20 years ago, ω_e could be measured, at least in principle, from

(1) line broadening,

(2) line shifts, or

(3) line narrowing.

All of these approaches have problems in applications, some of which are delineated on pp 49, 50, and 117−119 of the monograph.[1] In fact, in practice, the vast majority of the measurements relied on item 1, where the major problem at the time was the separation of concentration broadening effects due to spin exchange and dipolar interactions. The other two items 2 and 3 were thought to be interesting and important means to verify the theory[1] but in most cases impractical in applications to chemistry and biology. At the time of publication of the monograph,[1] there had not been a single case in which all three items 1−3 had been studied in the same system, and only two[1,10] cases combining items 1 and 2 and one[11] case combining items 1 and 3 had been studied. A critical review of the data shows that the quantitative aspects of the line shifts, item 2, were tested experimentally only twice.[1,10] One such test[10] was with aqueous solutions of peroxylamine disulfonate (Fremy's salt) where the theoretical predictions of a formalism equivalent to eq 1 but not written in that form were in agreement with experiment; another[1] test was with aqueous solutions of $VOSO_4$ where again theory and experiment agreed, however, with an experimental uncertainty of 50% of the shift. Thus, even though the theory[1] was thought to be complete, the experimental verification was scant indeed for items 2 and 3.

Recently, we decided to revisit the problem[2,7] to learn if line shifts rather than line broadening could be used in applications to chemistry and biology. Our interest arose because in micelles one observes a superposition of spectra due to those micelles containing one, two, and so forth spin probes, and the line width of this superposition is not very sensitive to ω_e. Our first effort[2] was to again work with aqueous solutions of Fremy's salt. Using modern understanding of line shapes,[12] computer fitting of spectra,[2,13] and significantly improved magnetic field and field sweep stabilities, we were able to reconfirm the theoretical prediction of the line shifts with high precision. In fact, ω_e could be measured from line shifts with a precision rivaling that found from line broadening. As an unexpected bonus to that work, we learned[2] that the distortions of the line shape from Lorentzian, predicted[1] from perturbation theory, were due to a spin-exchange-induced "dispersion". The sign of the dispersion term varies throughout the hyperfine multiplet and is zero for the central line if one exists.[2] Thus, each line is composed of an absorption and a dispersion component. Careful least-squares fitting of the lines to the two components yielded a new way to measure ω_e from

(4) the dispersion component.

Item 4 yielded values of ω_e that were also of precision comparable to the estimates derived from line broadening.[2] An advantage to item 4 is that a spectrum at $\omega_e = 0$ is not needed. As a corollary, the presence of spin exchange may be detected in a single spectrum.

With three ways to estimate the spin exchange in the slow exchange limit, items 1, 2, and 4, significant improvement in the reliability of the measurements could be achieved, and difficulties with any one method could be mitigated with the availability of the other two.

We next turned our attention[7] to a spin probe whose spectrum is severely inhomogeneously broadened by unresolved hyperfine structure, 16-doxylstearic acid methyl ester (16DSE). Our intention was to work out the details of treating the inhomogeneous broadening and to assess the accuracy with which ω_e could be measured using items 1, 2, and 4. This worked well for items 1 and 4; however, we were surprised[7] to find that the line shifts were no longer described by theory. An example of the magnitude of the discrepancies encountered is given in Figure 10, which reproduces some data from the previous work.[7] The discrepancies are substantial, and curiously the percent error increases as $\omega_e/A\gamma \rightarrow 0$. A search of the literature revealed that there were earlier indications that something was wrong with the theory. First Halpern et al.[14] and later Robinson et al.[15] observed line shifts that appeared to vary linearly with the concentration of the spin probe rather than quadratically as predicted by eq 1.

The present work was motivated by the following question: Why would the experimental shifts be in agreement with theory for Fremy's salt[2] and not for 16DSE?[7] An obvious difference is the presence of unresolved hyperfine structure in 16DSE and not in Fremy's salt; thus, we wondered if eq 1 did not correctly take into account the statistical factor, ρ_j. Earlier confirmations of the theoretical line shifts dealt exclusively with radicals with the same value of ρ_j for all of the lines. Perhaps eq 1 was correct for that case and incorrect if the values of ρ_j were not the same. At low values of ω_e, due to the superhyperfine interactions with the protons, 16DSE is a case in which the values of ρ_j are not the same. Here we study the nitronyl-nitroxide 1-*H*-imidazol-1-yloxy-4,5-dihydro-4,4,5,5-tetramethyl-2-(*o*-nitrophenyl)-3-oxide (NN-NP) in which the presence of two equivalent nitrogen nuclei gives five lines of different degeneracies $\rho_j = {}^1/_9{:}{}^2/_9{:}{}^3/_9{:}{}^2/_9{:}{}^1/_9$. Ullman and co-workers[16] discovered nitronyl-nitroxides and presented EPR spectra confirming the 1:2:3:2:1 expected relative intensities.

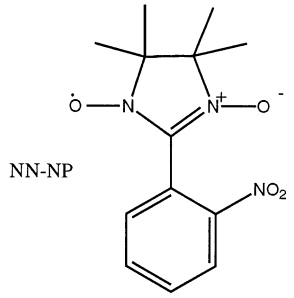

The purpose of the present work is threefold. First, we test eq 1 with inequivalent values of ρ_j. Second, we evaluate nitrones as prototypes to carry out spin-exchange applications in chemistry and biology. Finally, we apply a theory due to Salikhov[17] to explain the line shift results.

Theory

Molin et al.[1] applied second-order perturbation theory to eq 1 in the slow exchange limit, $\omega_e/\gamma A \ll 1$. The broadening of

TABLE 1: Line Broadenings and Line Shifts Predicted by Perturbation Theory for Two Equivalent ^{14}N Hyperfine Couplings[a]

	$M_I = \pm 2$	$M_I = \pm 1$	$M_I = 0$	eq
b_{M_I}	$\pm\frac{53\sqrt{3}}{72}\frac{B_0}{A}$	$\pm\frac{5\sqrt{3}}{9}\frac{B_0}{A}$	0	11
$H(\omega_e)^{abs}_{M_I} - H(0)_{M_I}$	$\pm\frac{1}{9}\frac{53}{64}\frac{B_0^2}{A}$	$\pm\frac{2}{9}\frac{10}{16}\frac{B_0^2}{A}$		12
$H(\omega_e)^{obs}_{M_I} - H(0)_{M_I}$	$\pm\frac{53}{64}\left[\frac{2}{3}\Delta H^L_{pp}(0)_{\pm 2} + B_0\right]\frac{B_0}{A}$	$\pm\frac{10}{16}\left[\frac{2}{3}\Delta H^L_{pp}(0)_{\pm 1} + B_0\right]\frac{B_0}{A}$		13
B_{M_I}	$\frac{4}{3}B_0$	$\frac{7}{6}B_0$	B_0	3
$V_{disp}(M_I)/V_{pp}(M_I)$	$\pm\frac{53}{54}\frac{B_0}{A}$	$\pm\frac{20}{27}\frac{B_0}{A}$	0	10

[a] All quantities written in terms of the broadening of the central line, $B_0 = 4\omega_e/3\sqrt{3}\gamma$.

the hyperfine line labeled with the nuclear quantum number M_I is given by

$$B_{M_I} = \frac{2\omega_e}{\sqrt{3}\gamma}(1 - \rho_{M_I}) \tag{3}$$

where ρ_{M_I} is the statistical weight of the M_I line and the broadening, B_{M_I}, is defined to be

$$B_{M_I} = \Delta H^L_{pp}(\omega_e)_{M_I} - \Delta H^L_{pp}(0)_{M_I} \tag{4}$$

The factor $(1 - \rho_{M_I})$ in eq 3 is the well-known probability that a spin probe will encounter another spin probe having a different value of M_I. For two equivalent ^{14}N nuclei, $\rho_{M_I} = (3 - |M_I|)/9$, yielding $(1 - \rho_{M_I}) = (6 + |M_I|)/9$. The broadening of the central line has the same numerical value as that found for spin probes with a single ^{14}N nucleus

$$B_0 = \frac{4\omega_e}{3\sqrt{3}\gamma} \tag{5}$$

whereas the inner and outer pairs of lines are predicted to show the broadenings detailed in Table 1, expressed in terms of B_0.

Previously,[2] we showed that the perturbation theory,[1] in first-derivative field-swept form, yielded a spectrum composed of absorption lines and spin-exchange-induced dispersion lines as follows:

$$Y'(H, \omega_e) = \sum_{M_I}[V_{pp}(M_I)\, L'_{M_I}(H) + V_{disp}(M_I)\, D'_{M_I}(H)] \tag{6}$$

In eq 6, $L'_{M_I}(H)$ is the first derivative of the absorption of Lorentzian line shape having unit peak-to-peak height given by

$$L'_{M_I}(H) = \frac{-8\xi'_{M_I}}{[3 + \xi'^2_{M_I}]^2} \tag{7}$$

whereas V_{pp} is the peak-to-peak amplitude of the first-derivative presentation. $D'_{M_I}(H)$ is the spin-exchange-induced dispersion of unit maximum amplitude given by

$$D'_{M_I}(H) = \frac{3[3 - \xi'^2_{M_I}]}{[3 + \xi'^2_{M_I}]^2} \tag{8}$$

and V_{disp} is its maximum amplitude. In eqs 7 and 8, ξ'_{M_I} is defined by

$$\xi'_{M_I} = 2\frac{H - H(\omega_e)_{M_I}}{\Delta H^L_{pp}(\omega_e)_{M_I}} \tag{9}$$

where $H(\omega_e)_{M_I}$ is the resonance field of the M_I line under the influence of spin exchange. To simplify the presentation, we use the term "dispersion" to mean the spin-exchange-induced dispersion terms in eq 6 and "instrumental dispersion" to mean the signal often arising from an incorrectly tuned microwave bridge.[18]

The amplitudes of the absorption and dispersion components in eq 6 calculated from the perturbation theory were shown to be related by[2]

$$V_{disp}(M_I)/V_{pp}(M_I) = 4\frac{\sqrt{3}b_{M_I}}{9} \tag{10}$$

where

$$b_{M_I} = -2(\omega_e/\gamma)\sum_{M_I' \neq M_I}\frac{\rho_{M_I'}}{H(0)_{M_I} - H(0)_{M_I'}} \tag{11}$$

In eq 11, the sum extends over all of the hyperfine lines other than M_I, and $H(0)_{M_I}$ denotes the resonance field of the M_I line in the absence of spin exchange. Table 1 lists values of b_{M_I} in the case of a five-line spectrum resulting from hyperfine coupling to two equivalent ^{14}N nuclei as well as the ratios $V_{disp}(M_I)/V_{pp}(M_I)$. Note, in particular, that the sign of b_{M_I} and thus of the ratio in eq 10 changes from positive on the low-field side of the center of the spectrum to negative on the high-field side.

There are two shifts of hyperfine lines in the perturbation theory.[1,2] The first, given as eq 22 of ref 2, is directly due to spin exchange and shifts the resonance frequencies of the lines toward the center

$$H(\omega_e)^{abs}_{M_I} - H(0)_{M_I} = \frac{1}{2}\rho_{M_I} b_{M_I}\omega_e/\gamma \tag{12}$$

The superscript "abs" refers to the resonance fields of the *absorption* lines. We showed in part 2 of this series[7] that inhomogeneous broadening does not affect the shifts as predicted by either eq 1 or the perturbation theory, eq 12.

The second shift is due to the overlap of the dispersion component. When this second shift is added to eq 12, we obtain the observed shift

$$H(\omega_e)^{obs}_{M_I} - H(0)_{M_I} = \frac{1}{2}\left(\frac{\sqrt{3}}{2}\Delta H^L_{pp}(0)_{M_I} + \frac{\omega_e}{\gamma}\right)b_{M_I} \tag{13}$$

The superscript "obs" refers to the resonance fields of the *observed* lines.

The positions $H(\omega_e)_{M_I}^{obs}$ are directly measurable from the EPR spectrum provided that the lines cross the baseline. The positions $H(\omega_e)_{M_I}^{abs}$ must be found by fitting the experimental spectrum to eq 6. The spacings $d_{in}^{abs}(\omega_e) = H(\omega_e)_{-1}^{abs} - H(\omega_e)_{+1}^{abs}$ and $d_{out}^{abs}(\omega_e) = H(\omega_e)_{-2}^{abs} - H(\omega_e)_{+2}^{abs}$ are conveniently measured from the line positions. The subscripts "in" and "out" denote the spacing between the *inner* pair of lines flanking the central line and the *outer* pair of lines flanking the central line, respectively. These spacings, which are defined in Figures 1 and 3, computed from eqs 12 and 13, and normalized to the spacing at $\omega_e = 0$, are given by

$$d_{out}^{abs}/d_{out} = 1 - \frac{1}{9}\frac{53}{128}\left(\frac{B_0}{A}\right)^2 \tag{14}$$

$$d_{in}^{abs}/d_{in} = 1 - \frac{2}{9}\frac{10}{16}\left(\frac{B_0}{A}\right)^2 \tag{15}$$

$$d_{out}^{obs}/d_{out} = 1 - \frac{53}{128}\left(\frac{2}{3B_0}\Delta H_{pp}^{L}(0)_{\pm 2} + 1\right)\left(\frac{B_0}{A}\right)^2 \tag{16}$$

$$d_{in}^{obs}/d_{in} = 1 - \frac{10}{16}\left(\frac{2}{3B_0}\Delta H_{pp}^{L}(0)_{\pm 2} + 1\right)\left(\frac{B_0}{A}\right)^2 \tag{17}$$

To simplify the notation, the dependence of the quantities on the left-hand side of eqs 14−17 on ω_e (manifested as B_0) is suppressed. For a single ^{14}N nucleus, the *observed* spacing was predicted (see eqs 25 and 26 of ref 2) to decrease more than 3 times faster than the *absorption* spacing. Here, the effect is amplified: the outer observed spacing decreases more than 9 times faster and the inner spacing decreases more than 4.5 times faster than the absorption spacings. Note that at $\omega_e = 0$ the observed and absorption spacings are the same because the dispersion lines are absent. Thus, d_{in} and d_{out} do not require superscripts.

Equations 14−17 are written in dimensionless form after having eliminated ω_e as a parameter using eq 3. Writing all results in terms of the broadening has the advantage that variations in concentration, temperature, or any other parameter that affects ω_e will automatically be accounted for provided that only spin exchange contributes to the broadening.

The doubly integrated intensity of each absorption line, I_{M_I}, may be calculated from the following equation,[2] which is valid for Lorentzian line shapes:

$$V_{pp}(M_I) = \sqrt{3} I_{M_I}/\pi[\Delta H_{pp}^{L}(\omega_e)_{M_I}]^2 \tag{18}$$

In part 2 of this series,[7] a serendipitous result emerged: even though eq 6 was derived[2] from perturbation theory and is valid only in the regime $\omega_e/A\gamma \ll 1$, the spectra, both simulated and experimental, could be fit to just two components per line, absorption and dispersion, to higher spin-exchange frequencies all the way up to line merger near $\omega_e/A\gamma \approx 1$ provided that the parameters B_{M_I}, $V_{disp}(M_I)/V_{pp}(M_I)$, and I_{M_I} are allowed to depart from the values predicted by perturbation theory. In other words, the form of eq 6 is valid all the way up to $\omega_e/A\gamma \approx 1$. One might have expected that, as $\omega_e/A\gamma$ increased, more and more terms would be needed in eq 6 to describe the spectrum, but this is not so. This fortunate fact allows us to describe the behavior of eq 1 in terms of the simple parameters B_{M_I}, $V_{disp}(M_I)/V_{pp}(M_I)$, and I_{M_I} all the way up to $\omega_e/A\gamma \approx 1$.

Materials and Methods

The nitronyl-nitroxide 1-*H*-imidazol-1-yloxy-4,5-dihydro-4,4,5,5-tetramethyl-2-(*o*-nitrophenyl)-3-oxide (NN-NP) was synthesized and purified essentially as previously described[19] with the exception that pure 2,3-dimethyl-2,3-dihydroxylaminobutane[20,21] (7.3 g; 41.5 mM) and 2-nitrobenzaldehyde (7.0 g; 46.3 mM) (Aldrich) were reacted in ethanol for 8 h at room temperature. After the oxidation and purification steps, NN-NP was obtained in 46% yield. UV λ_{max} (nm) [log ϵ]: 285 (s), 300 (s), 313 [4.190], 513 (s), 540.3 [3.202] (in water); 292 [3.991], 323 [4.041], 556 [2.948] (in ethanol); 582 [2.812] (in toluene). Further details are available in the Supporting Information.

A stock solution of NN-NP was prepared in distilled water at a concentration of approximately 5.9 mM. This solution was diluted to other intermediate concentrations of 5.8, 4.7, 3.5, 3.1, and 2.2 mM and two dilute solutions at 20 and 10 μM. The solutions, not degassed, were sealed with a gas−oxygen torch into 50 μL disposable pipets. As is well-known, dissolved oxygen broadens the EPR lines; however, the broadening due to spin exchange between NN-NP spin probes is independent of the presence of oxygen.[1] These pipets were housed in a quartz tube that was placed in the variable-temperature Dewar inside the microwave cavity. A thermocouple was placed above the sample in the same manner as that shown in configuration C of Figure 1 of ref 22. The sample temperature was stable to about ±0.1 °C during a spectrum sweep. Neither the concentration nor the temperature is a critical parameter in this work because both are removed as parameters by replacing ω_e by B_0 in eqs 14−17 and in the quantities in Table 1.

EPR spectra were measured with a Bruker 300 ESP X-band spectrometer interfaced with Bruker's computer. Spectra were acquired using a sweep time of 21 s, microwave power of 5 mW, time constant of 5 ms, sweep width of 50 G, and a modulation amplitude of 0.8 G. The broadening of the Gaussian component of the lines due to this modulation amplitude was corrected[23] as detailed below. The sweep width was measured by Bruker's NMR gaussmeter operating in the 1 mG resolution mode and was averaged over the entire experiment.

Equation 1 was generated using the equations in the appendix of part 1 of this series.[2]

Results

Low Concentration. Figure 1 shows the EPR spectrum of 20 μM NN-NP at 105 ± 1 °C. Each line was least-squares-fitted to a Gaussian−Lorentzian sum function,[12,13] from which the line position, overall line width, doubly integrated intensity, and Gaussian−Lorentzian sum function mixing parameter (parameter η of eq 13 of ref 12) were determined. The decomposition into the Gaussian and Lorentzian components of the approximately Voigt-shaped lines is described in refs 12 and 13. The lower trace is the experimental spectrum minus the five Gaussian−Lorentzian sum functions. Both the experimental spectrum and the residue hint at a minor impurity spectrum; however, carrying out the same procedure with 20 such spectra and summing failed to define the spectrum of a possible impurity. The only experimental parameter likely to be affected by the presence of a minor impurity spectrum is $V_{disp}(M_I)$ because this quantity is rather small and would be affected the most by an underlying impurity line. Fortunately,

TABLE 2: Hyperfine Spacings in the Absence of Spin Exchange (Gauss)

T, °C	$H_{+2} - H_{+1}$[a]	$H_{+1} - H_0$[a]	$H_0 - H_{-1}$[a]	$H_{-1} - H_{-2}$[a]	A[b]
-7.2 ± 0.2	8.096 ± 0.002	8.106 ± 0.002	8.084 ± 0.002	8.096 ± 0.004	8.0959 ± 0.0009
24.8 ± 0.2	8.084 ± 0.002	8.103 ± 0.001	8.079 ± 0.002	8.084 ± 0.002	8.0865 ± 0.0013
44.8 ± 0.4	8.078 ± 0.002	8.098 ± 0.002	8.076 ± 0.002	8.079 ± 0.002	8.0816 ± 0.0012
84.8 ± 0.7	8.060 ± 0.003	8.086 ± 0.004	8.064 ± 0.002	8.065 ± 0.005	8.0687 ± 0.0010
105 ± 1	8.055 ± 0.004	8.072 ± 0.004	8.056 ± 0.002	8.061 ± 0.002	8.0621 ± 0.0011

[a] Estimated error given by the standard deviation in five sweeps added to the manufacturers' stated accuracy in the NMR gaussmeter (±0.001 G). [b] Estimated error in the mean from two dilute samples weighted by their inverse variances.

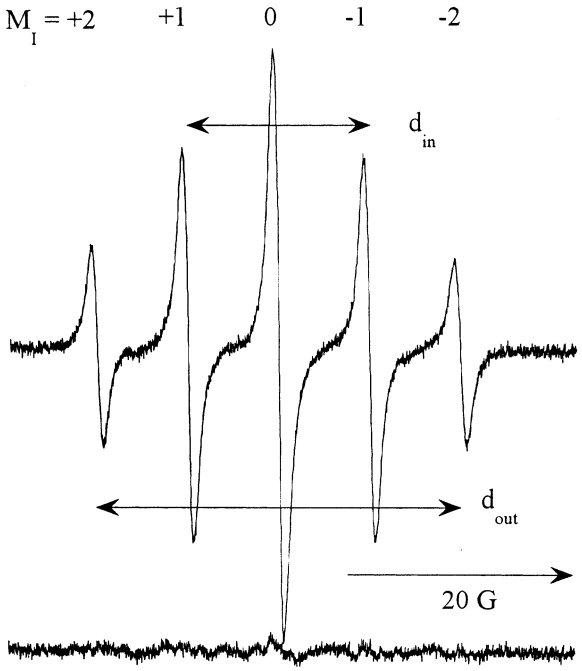

Figure 1. EPR spectrum of 20 μM NN-NP at 105 °C showing the definitions of the inner and outer spacings. The lower trace is the difference between the experimental spectrum and the best fit to five Gaussian−Lorentzian sum functions.

TABLE 3: Inner and Outer Spacings in the Absence of Spin Exchange and the Gaussian Line Widths (Gauss)

T, °C	d_{out}[a]	d_{in}[a]	ΔH_{pp}^{G}[b]	ΔH_{pp}^{G}[c]
-7.2 ± 0.2	32.383 ± 0.004	16.190 ± 0.002	0.793 ± 0.003	0.685
24.8 ± 0.2	32.346 ± 0.002	16.181 ± 0.001	0.758 ± 0.004	0.644
44.8 ± 0.4	32.326 ± 0.002	16.174 ± 0.002	0.746 ± 0.004	0.630
84.8 ± 0.7	32.275 ± 0.004	16.150 ± 0.002	0.708 ± 0.004	0.584
105 ± 1	32.248 ± 0.003	16.129 ± 0.003	0.700 ± 0.009	0.575

[a] Mean values and estimated errors in the means averaging five spectra from two dilute samples weighted by their inverse variances. [b] Mean values from five spectra for each hyperfine line were determined. These mean values were averaged, weighted by their inverse variances, over the five hyperfine lines. Errors are the estimated errors in the means. [c] Corrected for a field modulation amplitude of 0.8 G using ref 23.

we have some redundancy in the measurements of $V_{disp}(M_I)$, because we have five lines and $V_{disp}(M_I) = V_{disp}(-M_I)$.

Mean values and standard deviations of hyperfine spacings, Gaussian line widths, and Lorentzian line widths were found by fitting five spectra at each temperature for the two dilute samples. All values in the two samples were within their respective standard deviations of one another. This means that the values may be taken to correspond to $\omega_e = 0$ within experimental error. The results are detailed as follows: Table 2 gives the hyperfine spacings between adjacent hyperfine components. These are mean values of the means from the two dilute samples weighted by their inverse variances. Clearly, from Table 2, second-order shifts are easily measurable. These shifts are of no consequence in the present work; however, they are detailed in the Supporting Information. Table 3 gives the spacings d_{in} and d_{out} and the Gaussian line widths derived from the 20 μM sample. Also included in Table 3 are the Gaussian line widths corrected for the modulation broadening due to the modulation amplitude of 0.8 G as detailed in ref 23. Table 4 gives the values of the Lorentzian line widths derived from the 20 μM sample. The data in Tables 3 and 4 are changed insignificantly if the results from both dilute samples are properly averaged, weighting by the inverse variance of the respective mean values. This is because the uncertainties in the more dilute sample are significantly larger.

Higher Concentrations. The concentrations between 2.2 and 5.9 mM were studied at various temperatures between supercooled -7.2 ± 0.2 °C and superheated 105 ± 1 °C, yielding too much data to effectively present in the figures, so a representative selection of data of varying concentration and temperature are presented.

Figure 2a shows the experimental EPR spectrum of 4.7 mM NN-NP at 105 °C and, overlaid, the best fit of this spectrum to eq 6. These two curves are indistinguishable on the scale of Figure 2; the difference in them, multiplied by 10, is shown in Figure 2d. The absorption part of the best fit to eq 6 is shown in Figure 2b and the dispersion in Figure 2c. The fitted absorption curve, Figure 2b, is reproduced in Figure 3a, and the individual five absorption lines are detailed in Figure 3b−d. We emphasize that the parameters describing each line are varied independently in the least-squares fit. The spacings d_{in}^{abs} and d_{out}^{abs} are defined. See part 2 of this series[7] for more discussion of the fitting of broad spectra.

The best-fit dispersion curve in Figure 2c is reproduced in Figure 4a whereas the individual dispersion lines are detailed in Figure 4b−d. The dispersion apparent from the central line, Figure 4d, is due to a slightly improperly tuned bridge, which is often observed when employing lossy samples.[18] The values

TABLE 4: Lorentzian Line Widths[a] in the Absence of Spin Exchange (Gauss)

T, °C	$\Delta H_{pp}^{L}(0)_{+2}$	$\Delta H_{pp}^{L}(0)_{+1}$	$\Delta H_{pp}^{L}(0)_{0}$	$\Delta H_{pp}^{L}(0)_{-1}$	$\Delta H_{pp}^{L}(0)_{-2}$
-7.2 ± 0.2	0.305 ± 0.007	0.254 ± 0.010	0.234 ± 0.006	0.304 ± 0.005	0.417 ± 0.010
24.8 ± 0.2	0.341 ± 0.007	0.322 ± 0.008	0.317 ± 0.007	0.335 ± 0.007	0.376 ± 0.007
44.8 ± 0.4	0.407 ± 0.009	0.394 ± 0.007	0.388 ± 0.007	0.402 ± 0.007	0.428 ± 0.006
84.8 ± 0.7	0.590 ± 0.010	0.587 ± 0.007	0.579 ± 0.006	0.583 ± 0.007	0.604 ± 0.008
105 ± 1	0.670 ± 0.010	0.674 ± 0.010	0.669 ± 0.010	0.672 ± 0.010	0.694 ± 0.010

[a] From overall line widths using eq 7e of ref 12 employing the Gaussian line widths in Table 3. Errors are propagated in eq 7e using the standard deviations in overall line widths and the uncertainties in Table 3.

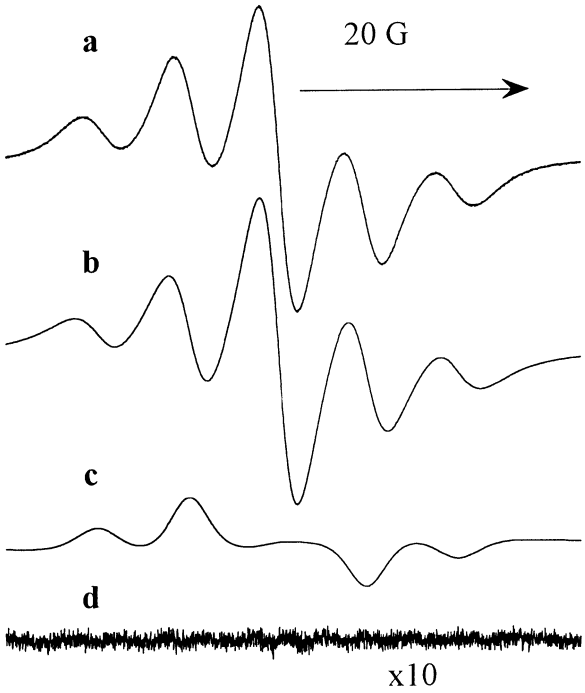

Figure 2. (a) Experimental EPR spectrum of 4.7 mM NN-NP at 105 °C. The best fit to eq 6 is indistinguishable from the experimental spectrum. (b) The absorption component of eq 6. (c) The spin-exchange-induced dispersion component of eq 6. (d) The difference between the experimental spectrum and the fit to eq 6, multiplied by 10.

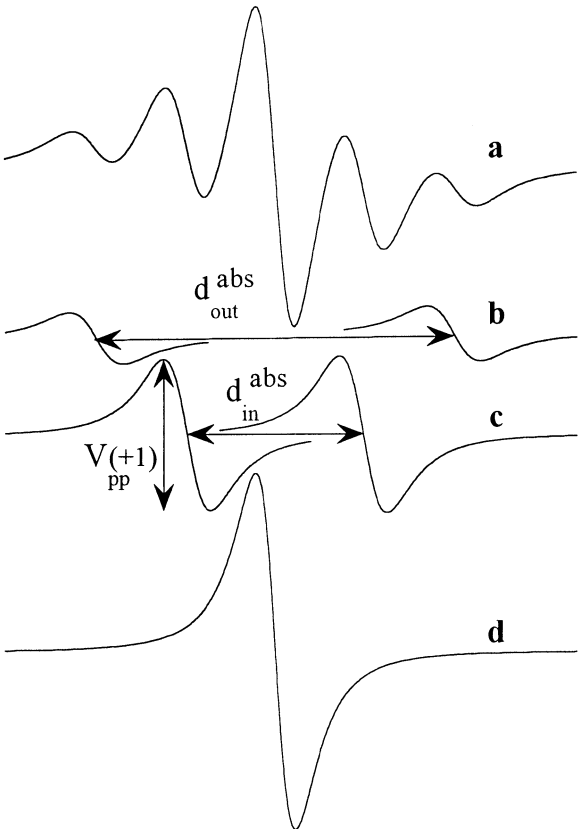

Figure 3. (a) The absorption component reproduced from Figure 2b. (b−d) Separated absorption lines that add to part a. The parameters of each of the five lines are varied independently to achieve a least-squares fit; those parameters are given in Table 5. The inner and outer absorption spacings as well as the peak-to-peak amplitude of one of the absorption lines are defined.

of $V_{disp}(M_I)/V_{pp}(M_I)$ for $M_I \neq 0$ are corrected for instrumental

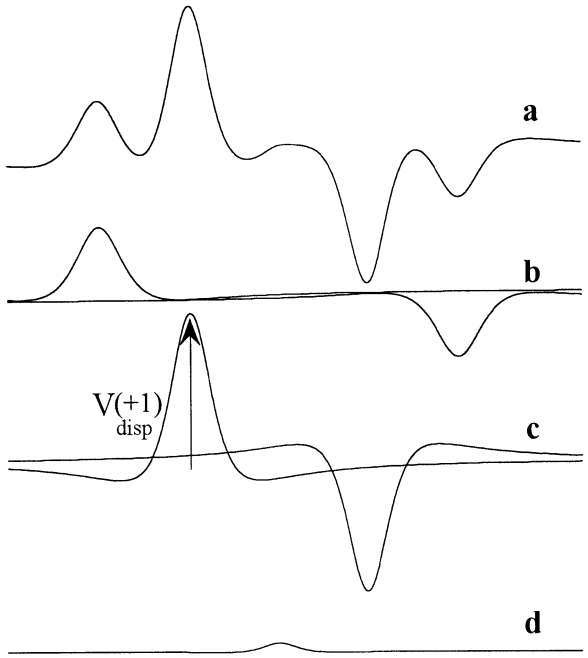

Figure 4. (a) The spin-exchange-induced dispersion component reproduced from Figure 2c. (b−d) Separated dispersion lines that add to part a. The parameters of each of the five lines are varied independently to achieve a least-squares fit and are listed in Table 5. The maximum amplitude of one of the dispersion lines is defined. The minor dispersion line for $M_I = 0$ (d) is due to instrumental dispersion which is used to correct the amplitudes of the other lines. See text.

dispersion by subtracting $V_{disp}(0)/V_{pp}(0)$ from each value of $V_{disp}(M_I)/V_{pp}(M_I)$ for $M_I \neq 0$.

To illustrate the quality of the fits, the detailed results for the spectrum in Figure 2 are presented in Table 5. Quoted uncertainties for individual results are the standard deviations in measurements of five spectra, one taken after the other. In Figures 5−8, each of the five measurements is plotted separately. From Table 5, it is concluded that all of the parameters are measured with high precision (reproducibility from five spectra), yet the accuracy of some parameters is lower, as can be judged by comparing the results for $M_I = \pm 2$ and for $M_I = \pm 1$. Thus, systematic errors are evident, especially for the quantities V_{disp}/V_{pp}. Column 4 of Table 5 gives values of ω_e/γ computed from eq 3; the ω_e/γ values in column 5 of Table 5 are computed from eq 44 (see the Appendix). The latter yields slightly more consistent results for ω_e.

Figure 2 illustrates that one may analyze spectra at significantly higher ratios of broadening to line spacing than was standard practice previously, $B/A < 0.3$.[4] For the outer lines, $B_{\pm 2}/A = 0.500$. Previously,[7] for 16DSE, we were able to analyze spectra to even larger values of ω_e, all the way up to spectral merging.[7] Regrettably, the solubility of NN-NP in water limited the range in this work.

In spectra such as those in Figure 2, where the broadening is large, the spacings d_{out}^{obs} and d_{out}^{obs} are not defined because the observed lines do not cross the baseline. In an application to chemistry or biology, assuming that results in the slow exchange region were of interest, the observed spacings would yield more precise results because the observed shifts are a factor of 9 (outside spacing) and 4.5 (inside spacing) larger than the absorption shifts. Further, they may be obtained without fitting. However, the observed shifts are less fundamentally related to the theory than absorption shifts because they include the overlap of the dispersion lines and involve the line widths at $\omega_e = 0$

TABLE 5: Results of Fitting the Spectrum in Figure 2 to Eq 6

M_I	ρ_{M_I}	B_{M_I},[a] G	ω_e/γ,[b] G	ω_e/γ,[c] G	V_{disp}/V_{pp}[a]	ω_e/γ,[d] G	I_{M_I}[e]	I_{M_I}[f]	I_{M_I}[g]
+2	1/9	4.034 ± 0.018	3.93	3.91	0.423 ± 0.005	4.05	0.254	0.333	0.260
+1	2/9	3.439 ± 0.007	3.83	3.82	0.326 ± 0.003	4.04	0.572	0.667	0.584
0	3/9	2.875 ± 0.002	3.73	3.81	0.008 ± 0.002		1.000	1.000	1.000
−1	2/9	3.489 ± 0.001	3.88	3.88	−0.275 ± 0.002	3.64	0.605	0.667	0.584
−2	1/9	3.968 ± 0.009	3.87	3.85	−0.349 ± 0.002	3.55	0.264	0.333	0.260
		mean	3.85 ± 0.075	3.85 ± 0.042		3.82 ± 0.26			

[a] Standard deviation from five spectra. [b] Equation 3. [c] Equation 44. [d] Equations 46 and 47 after correcting for nonzero $M_I = 0$ values. [e] Normalized to $I(0) = 1.000$. Standard deviation in five spectra ±0.001. [f] I_{M_I} from perturbation theory, normalized to $I(0) = 1.000$. [g] I_{M_I} from eq 45, normalized to $I(0) = 1.000$.

which can vary with M_I. Therefore, in the remainder of this paper we deal exclusively with d_{in}^{abs} and d_{out}^{abs}.

The perturbation theory predicts that the lines broaden according to eq 3, whereas eq 1 shows that the outer lines broaden slightly faster than this and the central line slightly slower. This is shown in Figure 5a where the line broadenings of theoretically generated lines from eq 1 are plotted versus the input value of $4\omega_e/3\sqrt{3}A\gamma$. These line broadenings are measured by fitting the theoretically generated spectra to eq 6 and are plotted as B_0/A, $3B_{\pm2}/4A$, and $6B_{\pm1}/7A$ to put them on the same scale according to eq 3. Perturbation theory predicts horizontal lines in Figure 5a; however, as before,[7] the outside lines broaden slightly faster than the perturbation theory prediction. The average normalized broadening, indicated by the ×'s, is defined to be

$$\langle B_0\rangle/A = [2(3B_{\pm2}/4A) + 2(6B_{\pm1}/7A) + B_0/A]/5 \quad (19)$$

and is within 0.0009 of unity up to a value of $4\omega_e/3\sqrt{3}\gamma = 0.375$. Thus, as before,[7] the average broadening is very nearly equal to the perturbation prediction even though the individual broadenings show departures. These departures were easily measurable in the case of 16DSE, where the range of ω_e/A was extended to about double the present range; however, in this work they are relatively minor, as is shown by the differences in the solid lines versus the dashed lines in Figure 5b. The dashed lines are the perturbation theory predictions, and the solid lines are from eq 1. The experimental values in Figure 5b were measured by fitting the data to an approximate Voigt function, neglecting dispersion, up to $\Delta H_{pp}^{L} = 2.4$ G and to a Lorentzian function including dispersion for $\Delta H_{pp}^{L} > 1.8$ G. This two-sided approach to deal with inhomogeneous broadening was discussed in detail in part 2 of this series.[7] Here, as before, the two approaches converge in the 1.8−2.4 G region (see Figure 3 of ref 7). The abscissa in Figure 5b is the experimental value of B_0/A whereas the circles correspond to the $M_I = \pm2$ lines and the squares to the $M_I = \pm1$ lines. The lower precision in the present work compared with that in the previous work with 16DSE is apparent when comparing Figure 5b with Figure 7 of ref 7. Nevertheless, it is clear that the difference in broadening of the hyperfine lines predicted by eq 3 is in accord with experiment, a result previously shown by Eastman and co-workers[24] for TCNE. By replacing B_0 with $\langle B_0\rangle$ in eqs 14−17, in Table 1, and in the abscissas of Figures 5−8, one arrives at a slightly more accurate representation, which is valid to high values of ω_e. In this work, the difference in B_0 and $\langle B_0\rangle$ is minor and is neglected in the abscissas of Figures 5b, 6, 7b, and 8.

Figure 6 displays the values of $V_{disp}(\pm2)/V_{pp}(\pm2)$, circles, and $V_{disp}(\pm1)/V_{pp}(\pm1)$, squares. Each data point is the average of the high- and low-field lines. The discrepancies in the values at high and lowfield are rather large, averaging ±6% for $M_I = \pm2$ and ±4% for $M_I = \pm1$. For the spectra in Figure 2, these discrepancies are ±7.5% and ±6%, respectively. The discrep-

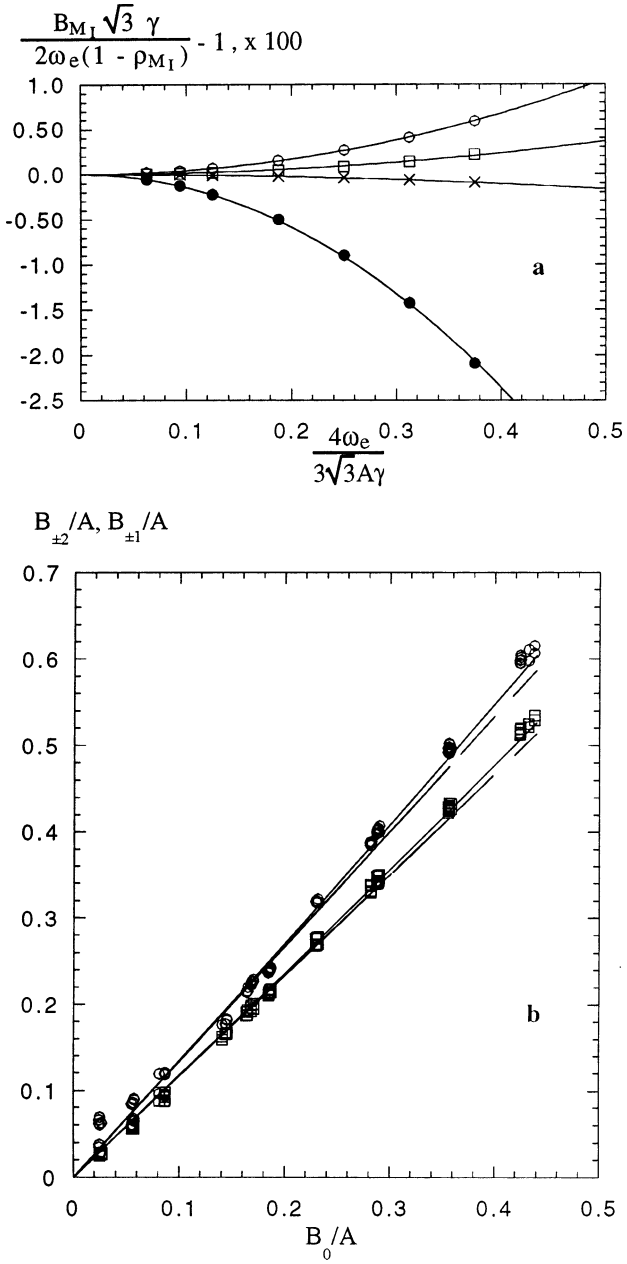

Figure 5. (a) Percent deviations of the line broadenings from the predictions of the perturbation theory, Table 1. The abscissa is the input value to eq 1 to generate a spectrum from which the line broadening is determined by least-squares fits. For $B_0^{input} = 4\omega_e/3\sqrt{3}\gamma$, values of $B_0/B_0^{input} - 1$ are denoted by ●, values of $3B_{\pm2}/4B_0^{input} - 1$ are denoted by ○, and values of $6B_{\pm2}/7B_0^{input} - 1$ are denoted by □. The average of the broadenings of all lines, calculated from eq 19, are denoted by ×. The outer lines broaden slightly faster than the perturbation theory prediction, and the central line broadens slightly more slowly. (b) Experimental values of B_{+2}/A (○), B_{-2}/A (○), B_{+1}/A (□), and B_{-1}/A (□) plotted versus the experimental value of B_0/A. The solid lines are from eq 1 containing no adjustable parameters; the dashed lines are from from perturbation theory, eq 3 of Table 1.

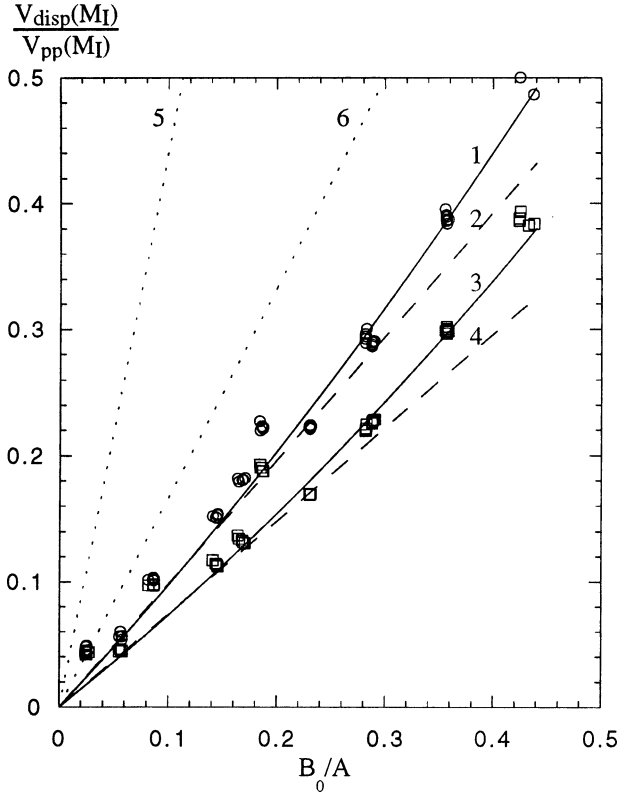

Figure 6. Experimental values of the average of V_{disp}/V_{pp} for $M_I = \pm 2$ (○) and $M_I = \pm 1$ (□). Solid lines 1 and 3 are the from eq 1 for $M_I = \pm 2$ and $M_I = \pm 1$, respectively, containing no adjustable parameters. Dashed lines 2 and 4 are from the perturbation theory, eq 10 of Table 1 for $M_I = \pm 2$ and $M_I = \pm 1$, respectively. Dotted lines 5 and 6 are from eq 5 of ref 25 for $M_I = \pm 2$ and $M_I = \pm 1$, respectively.

ancies are much larger than those encountered with 16DSE,[7] as is evident in Figure 8 of ref 7. Perhaps the source of this systematic error is a minor underlying impurity spectrum. The dashed lines 2 and 4 are the perturbation theory predictions, Table 1, and the solid lines 1 and 3 are derived by fitting spectra generated from eq 1. Nikonov and Nikonova[25] noted discrepancies in the line shifts predicted by eq 1 and experiment and advanced a theory to explain the discrepancies. The dotted lines 5 and 6, lying well above the measurements, are the predictions due to Nikonov and Nikonova,[25] showing that they are not in accord with experiment.

Figure 7a shows the differences between the theoretical values of I_{M_I}/ρ_{M_I} derived from eq 1 and the perturbation theoretical result of $I_{M_I}/\rho_{M_I} = 1$ plotted against the input value of $4\omega_e/3\sqrt{3}A\gamma$. The intensity of the central line, solid circles, grows at the expense of the $M_I = \pm 2$ lines, open circles, and of the $M_I = \pm 1$ lines, open squares. Figure 7b shows the experimental results for the $M_I = \pm 2$ and the $M_I = \pm 1$ lines normalized to the central line. Each data point is the average of the high- and low-field lines. The perturbation theory predicts the horizontal dashed lines at $^2/_3$ and $^1/_3$, and eq 1 is used to predict the solid lines. Equation 45 in the Appendix allows a corrected value of ω_e to be derived from the ratios. In the present case of five hyperfine lines, we observe, experimentally and theoretically, that intensity moves from the outer lines to the central line as ω_e increases.

We now turn to the first motivation of the present work in Figure 8, which shows d_{out}^{abs}/d_{out}, circles, and d_{in}^{abs}/d_{in}, squares, for data taken at 105 ± 1 °C. The predictions of perturbation theory are given by line 1 (eq 14) and line 2 (eq 15) for the outer and inner spacings, respectively. The small solid dots

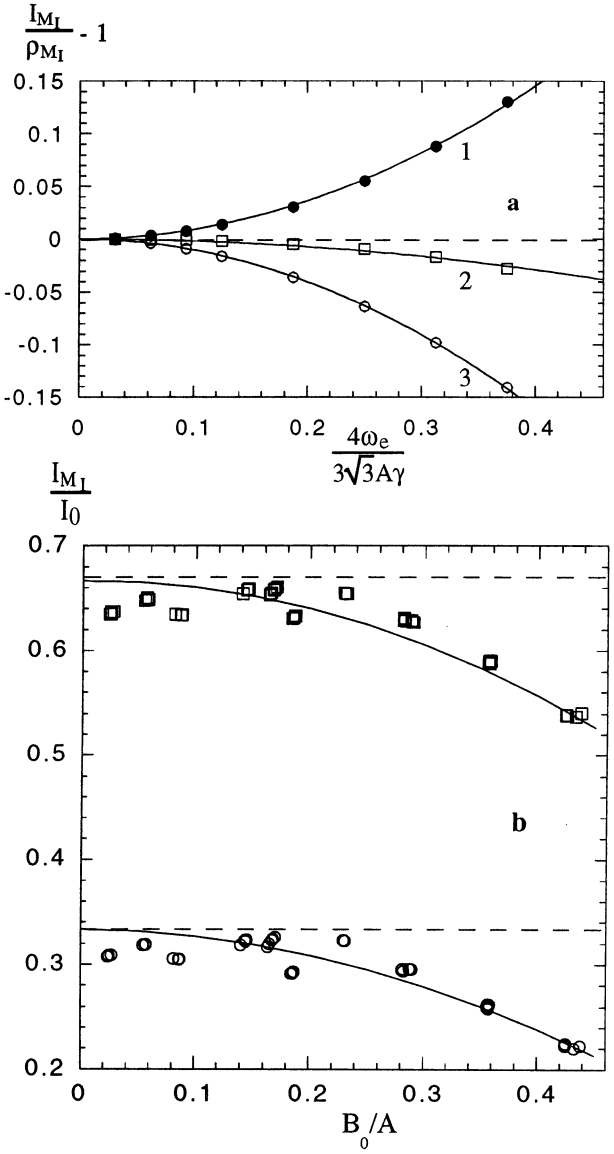

Figure 7. (a) Deviations of the values of the doubly integrated intensities of the lines from the perturbation theory prediction $I_{M_I}/\rho_{M_I} = 1$: line 1 (●), $M_I = 0$; line 2 (□), $M_I = \pm 1$; line 3 (○), $M_I = \pm 2$; dashed line, perturbation theory. The central line gains intensity at the expense of the other lines. (b) Experimental values of the average of I_{M_I}/I_0 for $M_I = \pm 2$ (○) and $M_I = \pm 1$ (□). The solid lines are from eq 1 containing no adjustable parameters; the dashed lines are from perturbation theory.

falling nearly coincident with lines 1 and 2 are derived from eq 1, showing that the full theory and the perturbation prediction are very nearly the same. This same result was noted before for the case of 16DSE[7] for three lines over even a larger range of ω_e. Clearly, here as before,[7] eq 1 and experiment are not in accord. Including inhomogeneous broadening in eq 1 or in eqs 14 and 15 by adding unresolved lines has no effect on the theoretical lines in Figure 8. Lines 3 and 4 are plots of the perturbation theory predictions each with an additional term linear in ω_e (manifested as $\langle B_0 \rangle/A$) as follows:

$$d_{out}^{abs}/d_{out} = 1 - \frac{1}{9}\frac{53}{128}\left(\frac{\langle B_0\rangle}{A}\right)^2 + \kappa_{out}\left(\frac{\langle B_0\rangle}{A}\right) \qquad (20)$$

$$d_{in}^{abs}/d_{in} = 1 - \frac{2}{9}\frac{10}{16}\left(\frac{\langle B_0\rangle}{A}\right)^2 + \kappa_{in}\left(\frac{\langle B_0\rangle}{A}\right) \qquad (21)$$

where $\kappa_{in} = -0.059 \pm 0.012$ and $\kappa_{out} = -0.053 \pm 0.002$ are

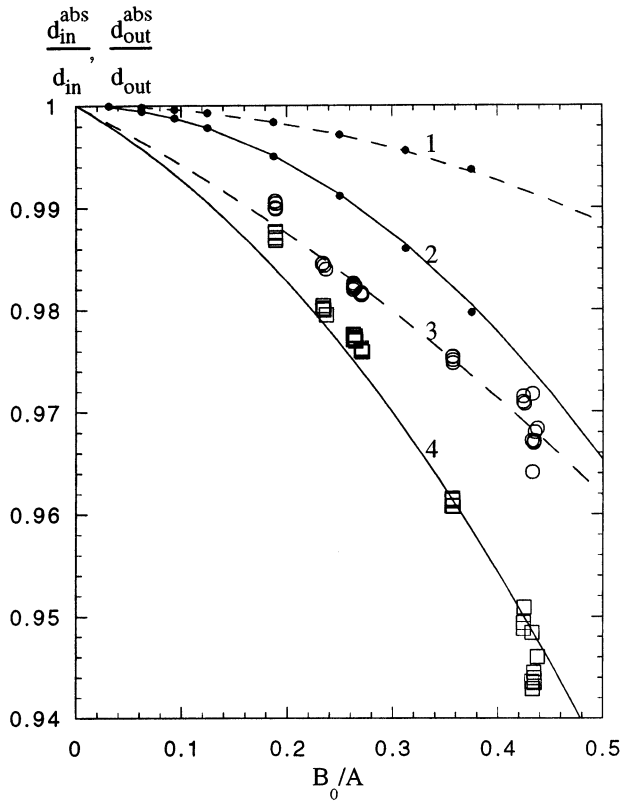

Figure 8. Experimental values of d_{out}^{abs}/d_{out} (○) and d_{in}^{abs}/d_{in} (□) at 105 °C: line 1, perturbation theory values of d_{out}^{abs}/d_{out} from eq 14; line 2, d_{in}^{abs}/d_{in} from eq 15, with or without unresolved proton hyperfine structure. The solid dots that are nearly coincident with lines 1 and 2 are derived from eq 1, with or without unresolved proton hyperfine structure. Lines 3 and 4 are linear least-squares fits to eqs 20 and 21, respectively.

constants adjusted to achieve a least-squares minimum between eqs 20 and 21 and the experimental data. If we plot (not shown) all of the data in this study, varying both the concentration and the temperature together, curves very similar to those in Figure 8 result and the fits to eqs 20 and 21 are of similar quality, yielding $\kappa_{in} = -0.060 \pm 0.002$ and $\kappa_{out} = -0.057 \pm 0.002$. Fitting all of the data to eqs 20 and 21 implies that κ_{in} and κ_{out} are assumed to be temperature independent.

Discussion

Despite the disappointing scatter in Figures 5−7, it is evident that experiment is in accord with eq 1, except for the line shifts. We emphasize that there are no adjustable parameters in the plots of eq 1. This confirms the correct dependence of eq 1 on ρ_{M_I}.

Apart from part 2 of this series[7] and the work by Nikonov and Nikonova,[25] we are aware of two previously reported discrepancies between experimentally observed line shifts and the predictions of perturbation theory. Halpern et al.[14] and later Robinson et al.[15] reported discrepancies in the sense that the line shifts varied linearly rather than quadratically with ω_e. Thus, qualitatively there were problems; however, these latter two groups did not compare experiment with theory quantitatively. In all three cases, the authors were dealing with *observed* line shifts rather than absorption shifts, although in Halpern et al.'s work,[14] there was very little difference between the two shifts due to small dispersion amplitudes. *Observed* line shifts do have a term linear in ω_e due to the overlap of the dispersion component, eq 13, whereas there is no such term in the expressions for the absorption shifts, eq 12. It is for this reason that we focus on the absorption shifts to eliminate the uncertainty involved in the additional shifts in the observed shifts due to dispersion overlap.

TABLE 6: Normalized Spacing = $1 - \Gamma(\langle B\rangle/A)^2 - \kappa(\langle B\rangle/A)$ [a]

	spacing	Γ	κ	κ [b]
^{15}N	A_{abs}/A	1.5	$0.866(\gamma A\tau_C + \sqrt{\gamma A\tau_D/2})$	0.19
^{14}N	$2A_{abs}/2A$	0.281	$0.650[\gamma A\tau_C + 0.805\sqrt{\gamma A\tau_D/2}]$	0.098
two ^{14}N	d_{out}^{abs}/d_{out}	0.0460	$0.650[\gamma A\tau_C + 0.650\sqrt{\gamma A\tau_D/2}]$	0.056
	d_{in}^{abs}/d_{in}	0.139	$0.650[\gamma A\tau_C + 0.729\sqrt{\gamma A\tau_D/2}]$	0.063

[a] $\langle B\rangle$ is the average broadening of the lines for ^{14}N and is $\langle B_0\rangle$ defined in eq 19 for two equivalent ^{14}N nuclei. [b] Evaluated with nominal values of $A = 22$ G for ^{15}N, 16 G for ^{14}N, 8 G for NN-NP, neglecting τ_C and using $\tau_D = 2.5 \times 10^{-10}$ s.

Note that we interpret the discrepancy between eq 1 and experiment as an additional linear term added to the predicted quadratic term rather than the previous suggestion[15] that the shifts are linear rather than quadratic.

Deviation of the Spin-Exchange-Induced Shifts from Theory. Equations 20 and 21 were introduced empirically in order to quantify the discrepancy between the perturbation theory predictions, eqs 14 and 15, and experiment; however, the existence of such a term had already been suggested in eq 2.142 in the monograph[1] and referred to by Robinson et al.[15] However, estimates of the parameters in eq 2.142[1] showed that the additional term is likely to be negligible in liquids of low viscosity. In the monograph,[1] eqs 1, 12, and 13 were derived under the assumption that spin exchange occurs instantaneously upon collision. This means that spin precession during the collision encounter is neglected. The problem was revisited by Salikhov[17] in 1985 who showed that, under conditions of strong exchange, not only spin precession during the collision encounter but also re-encounters lead to additional terms linear in ω_e. Thus, eqs 19 and 20 have the form of the theoretical predictions of Salikhov[17] if either spin precession during encounters, re-encounters, or both are included in the theory. The final result for strong exchange is given in eq 40 of ref 17 and involves both τ_C, the duration of one collision, and τ_D, the time between re-encounters. In the Appendix, we work out Salikhov's result[17] for NN-NP as well as for two- and three-line nitroxide spectra for reference. The results are summarized in Table 6. It was shown by Salikhov[17] that τ_C is most likely less than τ_D. Furthermore, the equations in the Appendix show that τ_C would have to be *larger* than τ_D to achieve the same shift. Thus, we neglect the terms involving τ_C, which yields, after evaluation of the numerical factors,

$$\kappa_{out} = -0.422\sqrt{\gamma A\tau_D/2} \tag{22}$$

and

$$\kappa_{in} = -0.474\sqrt{\gamma A\tau_D/2} \tag{23}$$

Inserting the experimental values of κ_{out} and κ_{in} into eqs 22 and 23 yields values of τ_D. Carrying out the analysis illustrated in Figure 8 for 105 °C at other temperatures yields values of τ_D which are plotted in Figure 9 versus η/T where η is the shear viscosity of water and T the absolute temperature. Separate estimates of τ_D are available from κ_{out} and κ_{in}, and these are in agreement with one another albeit with large error bars. Unfortunately, the analysis becomes of lower and lower precision as the temperature is decreased because the range of the abscissa of Figure 8 is decreased. Further, the accuracy of

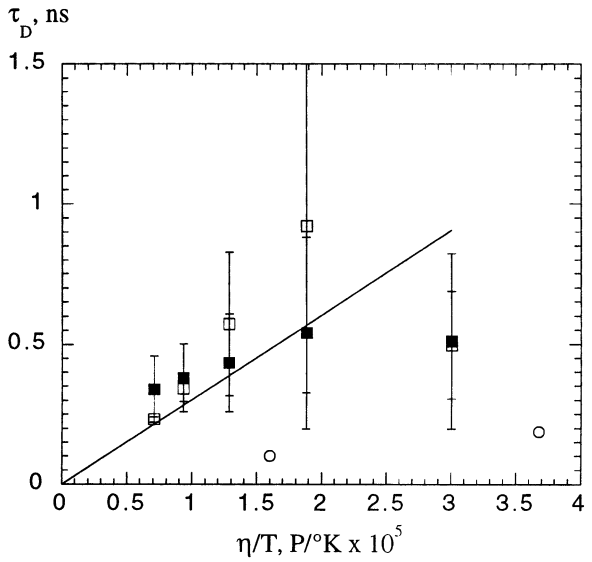

Figure 9. Mean time between re-encounters of NN-NP in water derived from eq 22 from the outer spacing (□) and from eq 23 from the inner spacing (■). The solid line is the Stokes−Einstein prediction, eq 25, for particles of radius 4.8 Å. Data for 16DSE in ethanol (○) are also shown.[7]

the results suffers because small uncertainties in the values of d_{in} and d_{out} become critical in the evaluation of κ_{out} and κ_{in}. To assess this latter uncertainty, we fit the data in two ways: fixing d_{in} and d_{out} to be the values in Table 3 or letting them be adjustable parameters in the fit to eqs 20 and 21. The two values of τ_D obtained from κ_{out} and κ_{in} were averaged, and the standard deviations are presented as the error bars in Figure 9.

We next turn to a crude theoretical estimate of the values of τ_D based on hydrodynamic theory. From the continuous diffusion model (see eq 32 of ref 17), the time between re-encounters between the same two particles in a single collision event is given by

$$\tau_D = b^2/D \tag{24}$$

where b is the interpartner separation of the two colliding particles, and D is the mutual diffusion coefficient. Estimating $D = 2D'$ with the Stokes−Einstein equation, where D' pertains to one particle, and setting b equal to twice the particle radius yield

$$\tau_D = \frac{3\pi b^3 \eta}{kT} \tag{25}$$

where k is the Boltzmann constant. We estimate $b = 9.6$ Å for NN-NP by setting the density of the molecule, assumed to be a sphere, equal to 1 g/cm^3. The solid line in Figure 9 is a plot of eq 25. Although Figure 9 appears to be consistent with a simple hydrodynamic model at higher temperatures, the large uncertainties prevent a definite conclusion from being drawn. In fact, the data in Figure 9 are also consistent with a constant value of τ_D, which explains the fact that all of the data, when both temperature and concentration are varied, can be fit to constant values of $\kappa_{in} = -0.060 \pm 0.001$ and $\kappa_{out} = -0.057 \pm 0.001$ which yield $\tau_D = 2.3 \times 10^{-10}$ and 2.6×10^{-10} s, respectively. The fact that Salikhov's theory[17] leads to values of τ_D similar to those derived from the inner and outer spacings lends support to the theory.

Figure 10 shows data for 16DSE in ethanol at 25 °C taken from part 2 of this series.[7] Line 1 is computed from perturbation theory,[7]

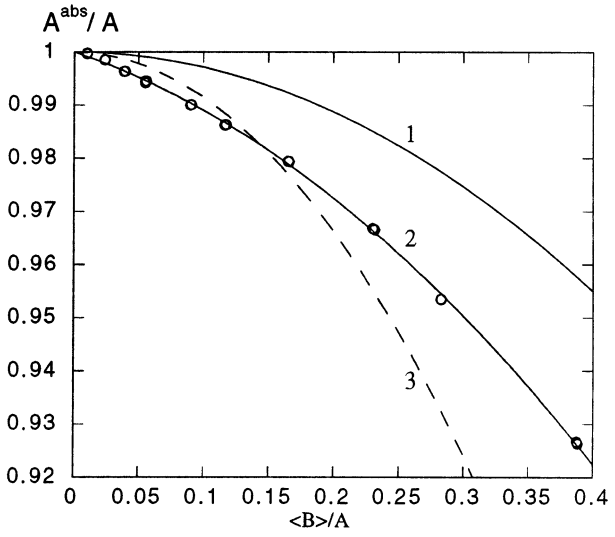

Figure 10. Experimental values of A^{abs}/A for 16DSE in ethanol at 25 °C taken from ref 7 (○): solid line 1, either from perturbation theory, eq 26, or from eq 1, with or without unresolved proton hyperfine structure; solid line 2, eq 27 including re-encounters; dashed line 3, eq 7 of Nikonov and Nikonova.[25]

$$A^{abs}/A = 1 - \frac{9}{32}\left(\frac{\langle B\rangle}{A}\right)^2 \tag{26}$$

where A^{abs} is one-half the separation between the low- and high-field lines of the three-line spectra and $\langle B\rangle$ is the average broadening from the three lines. The predicted curve from Nikonov and Nikonova's theory[25] is shown by the dashed line 3, demonstrating that it is an improvement over eq 1 at low values of ω_e but does not yield a satisfactory fit at high values. Further, the Nikonov and Nikonova[25] prediction for the dispersion height for 16DSE is 2.5 times too large.

Including re-encounters of the nitroxide moiety of 16DSE during a collision adds a term linear in ω_e, manifested as $\langle B\rangle/A$

$$A^{abs}/A = 1 - \frac{9}{32}\left(\frac{\langle B\rangle}{A}\right)^2 + \kappa(^{14}\mathrm{N})\left(\frac{\langle B\rangle}{A}\right) \tag{27}$$

Equation 27 yields the solid line 3 in Figure 10, where $\kappa_{16DSE} = -0.081 \pm 0.001$. The predicted linear term, Table 6, neglecting τ_C is given by

$$\kappa(^{14}\mathrm{N}) = -0.523\sqrt{\gamma A \tau_D/2} \tag{28}$$

Setting this equal to the experimental value and employing $A = 14.8$ G [7] yield $\tau_D = 1.9 \times 10^{-10}$ s, similar to the two estimates above for NN-NP. At 70 °C, the same treatment of the data yields $\tau_D = 1.0 \times 10^{-10}$ s. These two points are shown in Figure 9 as circles.

We resist speculating on the difference in the re-encounter times of NN-NP in water and 16DSE in ethanol until more data are available. We note that all of the re-encounter times in Figure 9 are consistent with Salikhov's estimate[17] of $\tau_D \sim 10^{-10}$ s. The fact that the data in Figure 9 depart from simple hydrodynamic theory is, in fact, encouraging. If τ_D were to simply follow the Stokes−Einstein equation, only the shear viscosity would be available, hiding potentially interesting physics that could distinguish the role of one liquid from another in the collision process. Perhaps, at last, spin exchange can lead to interesting insight into the collision process between two nitroxide spin probes.

The following comments on the uncertainties in Figure 9 may be helpful in planning future work. First, better spectra are needed, which probably means that a purer nitrone is needed. Second, to obtain accurate values of κ_{in} and κ_{out}, measurements need to be extended to rather large values of $\langle B_0 \rangle / A$, which requires that the nitrone be more soluble than NN-NP is in water. The use of a nitrone has the inherent advantage of the redundancy in the inner and outer spacings not to mention five sources of the broadening and four sources of the ratios V_{disp}/V_{pp}; however, it has the disadvantage that values of A are reduced by a factor of about 2 whereas the inhomogeneous broadening is about the same.

Table 6 shows that a perdeuterated ^{15}N spin probe holds, a priori, the greatest promise to measure τ_D because the expected values of κ are approximately a factor of 3 larger than those studied here. For these probes, however, one loses the redundancy mentioned in the previous paragraph. Probably the best approach would be to carry out parallel experiments with ^{14}N and ^{15}N isotopes of the same spin probe.

Finally we turn to the mystery of extra linear shifts in eqs 20, 21, and 27 for 16DSE and NN-NP as well as those spin probes employed by Robinson et al.,[15] Halpern et al.,[14] and Nikonov and Nikonova[25] and the absence of such shifts[2] in Fremy's salt. It was not appreciated at first,[1] but was clarified later by Salikhov,[17] that the additional linear shifts are very small, perhaps even negative (lines move away from the spectral center) in the case of intermediate strength exchange interactions, $J\tau_C \approx 1$. Eastman and co-workers[5] proposed that an aqueous solution of Fremy's salt was just such a case; thus, an additional linear term would not be expected.[17] Therefore, the puzzle of why Fremy's salt did not exhibit[2,10] an extra linear shift could be explained by Salikhov's theory[17] as being due to the difference in the strength of the spin-exchange interaction. We should point out that Eastman and co-workers'[5] interpretation of $J\tau_C \approx 1$ has been questioned (see p 198 of ref 1). Careful measurement of line shifts might shed light on the strength of the exchange interaction in other cases in which there is doubt. For example, consider the data in Figure 4.3 of the monograph.[1]

Salikhov[17] suggested that separation of the contribution of line shifts due to spin motion during an encounter could be informative concerning spin dynamics. This work shows that this separation might be possible, although it may not be easy. This would be very interesting indeed because spin exchange in liquids, as studied by line broadening, has turned out to be less informative about liquid dynamics than had been hoped because the shear viscosity of the liquid dominates the value of ω_e, making it difficult to learn anything about the collision act itself. It should be emphasized that access to the rather small line shifts must be via least-squares fitting to reasonable line shapes; it is very unlikely that measurements of simple parameters derived from a few points on the experimental spectra will be fruitful.

Conclusions

Equation 1 may be represented by the sum of five absorption and five spin-exchange-induced dispersion lines at all values of ω_e. Equation 1 is in agreement with all aspects of the spectral changes induced by spin exchange except for the line shifts. These changes include the following: (1) the central line broadens slightly more slowly and the other four lines slightly more rapidly than predicted by perturbation theory (Figure 5); (2) intensity is transferred to the central line from the other four lines (Figure 7); (3) the spin-exchange-induced dispersion lines grow more rapidly than the perturbation result (Figure 7). There are no adjustable parameters in the comparison of experiment with eq 1. An alternative perturbation treatment due to Nikonov and Nikonova[25] is found not to be in agreement with experiment. Including in the theory the effects of re-encounters of the same spins during collision introduces line shifts that are in addition to those of eq 1 and vary linearly with ω_e. These additional line shifts depend on one additional parameter, the mean time between re-encounters, τ_D. The total line shifts are in agreement with experiment using reasonable values of τ_D.

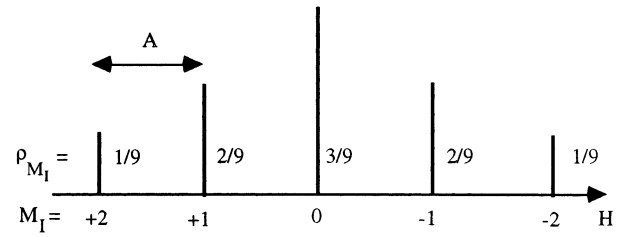

Figure 11. Stick diagram of the hyperfine pattern of NN-NP showing the hyperfine spacing in the absence of spin exchange, A, and the statistical factors ρ_{M_I}.

Acknowledgment. The authors gratfully acknowledge support from NIH Grants 5 S06 GM48680-09 and 3S06 GM048680-10S1.

Appendix

Additional Shifts due to Spin Precession during Encounters and Re-encounters. The additional field shifts of the kth line due to spin precession during encounters and re-encounters, under conditions of strong exchange, are given by eq 40 of Salikhov[17]

$$\delta'_k = -\frac{1}{2}\frac{\omega_e}{\gamma}\sum \rho_n x_{nk} \tag{29}$$

where $K_D C$ in the orginal publication[17] has been set equal to $2\omega_e$ and a steric factor has been set equal to unity. The sum in eq 29 extends over all lines except the kth, and γ converts the expression to magnetic field units. The prime in δ'_k means that this shift is in addition to the normal shifts, that is, those in eq 1 (or, with negligible error, eq 12). The quantity x_{nk} is given by

$$x_{nk} = (\omega_k - \omega_n)\tau_C + \mathrm{sign}(\omega_k - \omega_n)\sqrt{|(\omega_k - \omega_n)|\tau_D/2} \tag{30}$$

Additional Shifts of Outer Lines. See Figure 11 for a schematic of the spectrum. Take k to be $M_I = +2$ to get the additional shift of the low-field line. The sum has four terms as n assumes the values of $M_I = +1$, 0, -1, and -2. For these values of M_I, $(\omega_k - \omega_n)$ assumes values of $-\gamma A$, $-2\gamma A$, $-3\gamma A$, and $-4\gamma A$, respectively, and $-\rho_n x_{nk}$ assumes the values of $^2/_9[\gamma A\tau_C + \sqrt{\gamma A\tau_D/2}]$, $^3/_9[\gamma 2A\tau_C + \sqrt{\gamma 2A\tau_D/2}]$, $^2/_9[\gamma 3A\tau_C + \sqrt{\gamma 3A\tau_D/2}]$, and $^1/_9[\gamma 4A\tau_C + \sqrt{\gamma 4A\tau_D/2}]$, respectively. The sum of these yield

$$\sum \rho_n x_{nk} = -[2\gamma A\tau_C + C_{out}\sqrt{\gamma A\tau_D/2}] \tag{31}$$

where $C_{out} = (2 + 3\sqrt{2} + 2\sqrt{3} + 2)/9 = 1.30$. Thus, the low-field line shifts by

$$\delta'_{+2} = \frac{1}{2}\frac{\omega_e}{\gamma}[2\gamma A\tau_C + C_{out}\sqrt{\gamma A\tau_D/2}] \tag{32}$$

The high-field line shifts an amount equal and opposite, so the outer line spacing divided by its value at $\omega_e = 0$, $d_{out} = 4A$ (ignoring small second-order shifts), has the additional term

$$-2\frac{1}{2}\frac{\omega_e}{\gamma}[2\gamma A\tau_C + C_{out}\sqrt{\gamma A\tau_D/2}]/4A \quad (33)$$

Substituting $\langle B_0\rangle = 4\omega_e/3\sqrt{3}\gamma$ and adding to eq 14 yield eq 20 with

$$\kappa_{out} = -\frac{3\sqrt{3}}{16}[2\gamma A\tau_C + C_{out}\sqrt{\gamma A\tau_D/2}] \quad (34)$$

Additional Shifts of Inner Lines. Now take k to be $M_I = +1$ to get the shift of that line. The sum in eq 29 has four terms as n assumes the values of $M_I = +2$, 0, -1, and -2. For these values of M_I, $(\omega_k - \omega_n)$ assumes the values of $+\gamma A$, $-\gamma A$, $-2\gamma A$, and $-3\gamma A$, respectively, and $-\rho_n x_{nk}$ assumes the values of $-{}^1/_9[\gamma A\tau_C + \sqrt{\gamma A\tau_D/2}]$, ${}^3/_9[\gamma A\tau_C + \sqrt{\gamma A\tau_D/2}]$, ${}^2/_9[\gamma 2A\tau_C + \sqrt{\gamma 2A\tau_D/2}]$, and ${}^1/_9[\gamma 3A\tau_C + \sqrt{\gamma 3A\tau_D/2}]$, respectively. The sum of these yield

$$\sum \rho_n x_{nk} = -[\gamma A\tau_C + C_{in}\sqrt{\gamma A\tau_D/2}] \quad (35)$$

where $C_{in} = (2 + 2\sqrt{2} + \sqrt{3})/9 = 0.729$. Thus, the $M_I = +1$ line shifts by

$$\delta'_{+1} = \frac{1}{2}\frac{\omega_e}{\gamma}[\gamma A\tau_C + C_{in}\sqrt{\gamma A\tau_D/2}] \quad (36)$$

The $M_I = -1$ line shifts by the same amount in the opposite direction, so, following the same procedure as above, we find

$$\kappa_{in} = -\frac{3\sqrt{3}}{8}[\gamma A\tau_C + C_{in}\sqrt{\gamma A\tau_D/2}] \quad (37)$$

Additional Shifts of Three Lines, ^{14}N. Here, there are two terms in the sum of eq 29. Carrying out the same calculations shows that the line spacing divided by its value at $\omega_e = 0$, A, has the additional term

$$-\frac{1}{2}\frac{\omega_e}{\gamma}\left(\gamma A\tau_C + \frac{1}{3}(1+\sqrt{2})\sqrt{\gamma A\tau_D/2}\right)/A \quad (38)$$

Substituting $\omega_e = 3\sqrt{3}\gamma\ \langle B\rangle/4$, where $\langle B\rangle$ is the average broadening of the three lines, and adding this shift to the "normal" shift, eq 26, yield eq 27 with

$$\kappa(^{14}\mathrm{N}) = -\frac{3\sqrt{3}}{8}\left[\gamma A\tau_C + \frac{1}{3}(1+\sqrt{2})\sqrt{\gamma A\tau_D/2}\right] \quad (39)$$

Additional Shifts of Two Lines, ^{15}N. Here, for the $M_I = +{}^1/_2$ line, there is one term in the sum of eq 29. Carrying out the same calculations shows that the line spacing divided by its value at $\omega_e = 0$, A, has the additional term

$$-\frac{1}{2}\frac{\omega_e}{\gamma}[\gamma A\tau_C + \sqrt{\gamma A\tau_D/2}]/A \quad (40)$$

The "normal" shift of ^{15}N lines computed from eq 12 yields a spacing of

$$A^{abs}/A = 1 - \frac{3}{2}\left(\frac{B}{A}\right)^2 \quad (41)$$

Substituting $B = \omega_{ex}/\sqrt{3}\gamma$ into eq 40 and adding to eq 41 yield

$$A^{abs}/A = 1 - \frac{3}{2}\left(\frac{B}{A}\right)^2 + \kappa(^{15}\mathrm{N})\left(\frac{B}{A}\right) \quad (42)$$

with

$$\kappa(^{15}\mathrm{N}) = -\frac{1}{2}\sqrt{3}(\gamma A\tau_C + \sqrt{\gamma A\tau_D/2}) \quad (43)$$

Table 6 gives a summary of the total shifts due to spin exchange for the three cases considered here with the numerical factors computed for easy comparison. It is clear that the normal shifts (quadratic in ω_e, with coefficient Γ) vary considerably depending on the spin probe employed. The inner versus the outer shift in NN-NP also varies considerably. The extra shifts, κ, vary more modestly from probe to probe. The final column of Table 6 gives the value of κ employing typical hyperfine coupling constants, neglecting τ_C, and using a typical value of $\tau_D = 2.5 \times 10^{-10}$ s.

Deviations of Perturbation Theory from Equation 1. *Broadening.* Figure 5a shows that the broadening according to eq 1 is slightly different from that predicted by perturbation theory, eq 3. The solid lines are approximated with negligible error by the following:

$$\frac{B_{M_I}\sqrt{3}\gamma}{2\omega_e(1-\rho_{M_I})} = 1 + \lambda_{M_I}\left\{\frac{4\omega_e}{3\sqrt{3}A\gamma}\right\}^2 \quad (44)$$

with $\lambda_0 = -0.147$, $\lambda_{\pm1} = +0.015$, and $\lambda_{\pm2} = +0.042$ from which a corrected value of ω_e may be obtained.

Intensities. Figure 7a shows that the intensities vary substantially from the perturbation theory prediction $I_{M_I} = \rho_{M_I}$. The solid lines are given as follows:

$$\frac{I_{M_I}}{\rho_{M_I}} = 1 + \xi_{M_I}\left\{\frac{4\omega_e}{3\sqrt{3}A\gamma}\right\}^2 \quad (45)$$

with $\xi_0 = +0.911$, $\xi_{\pm1} = -0.180$, and $\xi_{\pm2} = -1.01$. It is clear that, in principle, ω_e can be estimated from the variation of the intensities. Applying eq 45 to the data in column 8 of Table 5 yields $\omega_e/\gamma = 3.70 \pm 0.38$. Because of the large uncertainty, intensity variations serve more as a consistency check than a viable method to measure ω_e.

Dispersion Amplitudes. The solid lines in Figure 6 are given as follows:

$$\left|\frac{V_{disp}(\pm2)}{V_{pp}(\pm2)}\right| = \frac{53}{54}\left\{\frac{4\omega_e}{3\sqrt{3}A\gamma}\right\}\left(1 + 0.631\left\{\frac{4\omega_e}{3\sqrt{3}A\gamma}\right\}^2\right) \quad (46)$$

$$\left|\frac{V_{disp}(\pm1)}{V_{pp}(\pm1)}\right| = \frac{20}{27}\left\{\frac{4\omega_e}{3\sqrt{3}A\gamma}\right\}\left(1 + 0.777\left\{\frac{4\omega_e}{3\sqrt{3}A\gamma}\right\}^2\right) \quad (47)$$

Line Spacing. Amazingly, the values of the line spacings predicted by eq 1 and by perturbation theory are not significantly different as shown by Figure 8. For example, the differences in d^{abs}_{out}/d_{out} and d^{abs}_{in}/d_{in} from eq 1 versus eqs 14 and 15 are only 2×10^{-4} and 0.8×10^{-4}, respectively, at $4\omega_e/3\sqrt{3}A\gamma = 0.375$, a negligible difference compared with the additional linear term needed in eqs 20 and 21.

Supporting Information Available: Further details on the synthesis of NN-NP as well as details on the second-order shifts in the absence of spin exchange are available. This material is available free of charge via the Internet at http://pubs.acs.org.

References and Notes

(1) Molin, Y. N.; Salikhov, K. M.; Zamaraev, K. I. *Spin Exchange. Principles and Applications in Chemistry and Biology*; Springer-Verlag: New York, 1980.

(2) Bales, B. L.; Peric, M. *J. Phys. Chem. B* **1997**, *101*, 8707.
(3) Edelstein, N.; Kwok, A.; Maki, A. N. *J. Chem. Phys.* **1964**, *41*, 3473.
(4) Plachy, W.; Kivelson, D. *J. Chem. Phys.* **1967**, *47*, 3312.
(5) Eastman, M. P.; Bruno, G. V.; Freed, J. H. *J. Chem. Phys.* **1970**, *52*, 2511.
(6) Berner, B.; Kivelson, D. *J. Phys. Chem.* **1979**, *83*, 1406.
(7) Bales, B. L.; Peric, M. *J. Phys. Chem. A* **2002**, *106*, 4846.
(8) Currin, J. D. *Phys. Rev.* **1962**, *126*, 1995.
(9) Kivelson, D. *J. Chem. Phys.* **1960**, *33*, 1094.
(10) Jones, M. T. *J. Chem. Phys.* **1963**, *38*, 2892.
(11) Miller, T. A.; Adams, R. N.; Richards, P. M. *J. Chem. Phys.* **1966**, *44*, 4022.
(12) Bales, B. L. In *Biological Magnetic Resonance*; Berliner, L. J., Reuben, J., Eds.; Plenum Publishing Corporation: New York, 1989; p 77.
(13) Halpern, H. J.; Peric, M.; Yu, C.; Bales, B. L. *J. Magn. Reson.* **1993**, *103*, 13.
(14) Halpern, H. J.; Peric, M.; Nguyen, T.-D.; Teicher, B. A.; Lin, Y. J.; Bowman, M. K. *J. Magn. Reson.* **1990**, *90*, 40.
(15) Robinson, B. H.; Mailer, C.; Reese, A. W. *J. Magn. Reson.* **1999**, *138*, 210.
(16) Ullman, E. F.; Osiecki, J. H.; Boocock, D. G. B.; Darcy, R. *J. Am. Chem. Soc.* **1972**, *94*, 7049.
(17) Salikhov, K. M. *J. Magn. Reson.* **1985**, *63*, 271.
(18) Ludowise, P.; Eaton, S. S.; Eaton, G. R. *J. Magn. Reson.* **1991**, *93*, 410.
(19) Dragutan, I.; Dragutan, V.; Caragheorgheopol, A.; Zarkadis, A. K.; Fischer, H.; Hoffmann, H. *Colliods Surf., A* **2001**, *183*−*185*, 767.
(20) Ovcharenko, V. I.; Fokin, S. V.; Rey, P. *Mol. Cryst. Liq. Cryst. Sci. Technol., Sect. A* **1999**, *334*, 109.
(21) Ovcharenko, V. I.; Fokin, S. V.; Romanenko, G. V.; Korobkov, I. V.; Rey, P. *Russ. Chem. Bull.* **1999**, *48*, 1519.
(22) Bales, B. L.; Wajnberg, E.; Nascimento, O. R. *J. Magn. Reson.* **1996**, *A118*, 227.
(23) Bales, B. L.; Peric, M.; Lamy-Freund, M. T. *J. Magn. Reson.* **1998**, *132*, 279.
(24) Eastman, M. P.; Kooser, R. G.; Das, M. R.; Freed, J. H. *J. Phys. Chem.* **1969**, *71*, 38.
(25) Nikonov, A. M.; Nikonova, S. I. *Sov. J. Chem. Phys.* **1991**, *7*, 2408.